NEURO CRITICAL
CARE SOCIETY

SPREADING CORTICAL DEPOLARIZATION

Cortical Spreading Depolarizations in a Mouse Model of Subarachnoid Hemorrhage

Check for updates

James H. Lai[1,2], Tao Qin[1], Sava Sakadžić[3], Cenk Ayata[1,4] and David Y. Chung[1,2]*

Abstract

Background: Cortical spreading depolarizations (CSDs) are associated with worse outcomes in patients with aneurysmal subarachnoid hemorrhage (SAH). Animal models are required to assess whether CSDs can worsen outcomes or are an epiphenomenon; however, little is known about the presence of CSDs in existing animal models. Therefore, we designed a study to determine whether CSDs occur in a mouse model of SAH.

Methods: A total of 36 mice were included in the study. We used the anterior prechiasmatic injection model of SAH under isoflurane anesthesia. A needle was inserted through the mouse olfactory bulb with the point terminating at the base of the skull, and arterial blood or saline (100 μl) was injected over 10 s. Changes in cerebral blood volume over the entire dorsal cortical surface were assessed with optical intrinsic signal imaging for 5 min following needle insertion.

Results: CSDs occurred in 100% of mice in the hemisphere ipsilateral to olfactory bulb needle insertion (CSD1). Saline-injected mice had 100% survival ($n = 10$). Blood-injected mice had 88% survival ($n = 23$ of 26). A second, delayed, CSD ipsilateral to CSD1 occurred in 31% of blood-injected mice. An increase in the time interval between CSD1 and blood injection was associated with the occurrence of a second CSD in blood-injected mice (mean intervals 26.4 vs. 72.7 s, $p < 0.0001$, $n = 18$ and 8). We observed one blood-injected animal with a second CSD in the contralateral hemisphere and observed terminal CSDs in mice that died following SAH injection.

Conclusions: The prechiasmatic injection model of SAH includes CSDs that occur at the time of needle insertion. The occurrence of subsequent CSDs depends on the timing between CSD1 and blood injection. The mouse prechiasmatic injection model could be considered an SAH plus CSD model of the disease. Further work is needed to determine the effect of multiple CSDs on outcomes following SAH.

Keywords: Brain aneurysm, Cortical spreading depression, Delayed cerebral ischemia, Neurocritical care, Mouse model

Introduction

Subarachnoid hemorrhage (SAH) from a ruptured brain aneurysm is a complex disease with a wide range of clinical presentations and injury severity [1–3]. Functional outcome has been associated with the degree of early brain injury and onset of a syndrome of delayed neurological decline [4, 5]. Sources of brain injury burden are thought to be multifactorial and include global ischemia at the time of aneurysm rupture, inflammation, and delayed arterial vasospasm. Furthermore, there is a body of evidence demonstrating that cortical spreading depolarizations (CSDs) are associated with worse outcomes in patients with SAH [6]; however, additional experimental work is required to establish a causal relationship between CSDs and patient outcomes after SAH [7].

*Correspondence: dychung@mgh.harvard.edu
[1] Neurovascular Research Unit, Department of Radiology, Massachusetts General Hospital, Harvard Medical School, 149 13th St, Charlestown, MA 02129, USA
Full list of author information is available at the end of the article

This article is part of the collection on "Spreading Cortical Depolarization".

Springer

Animal models have been helpful in elucidating the role of CSDs in migraine aura and ischemic stroke [8, 9] and will likely be essential for explicating the role of CSDs in the pathogenesis of SAH. Mouse models, in particular, have special advantages given their relative ease of genetic manipulation, cost, and the breadth of behavioral assessments available. There have been no observations of early or delayed spontaneous CSDs reported in any of the mouse models of SAH [10]. Therefore, we designed the current study to determine whether CSDs occur in a mouse model of SAH during the peri-induction period.

Methods

Animals

We followed the Animal Research: Reporting of In Vivo Experiments (ARRIVE) guidelines 2.0 for reporting of animal research as applicable with exceptions noted [11]. Animal protocols were approved by the Institutional Animal Care and Use Committee (Massachusetts General Hospital Subcommittee on Research Animal Care). Mice were kept in an American Association for Accreditation of Laboratory Animal Care (AAALAC)-accredited animal facility in cage groups of two to four with diurnal lighting, room temperature of 25 °C, and air humidity of 45–65%. Sample sizes for blood- or saline-injected mice were determined empirically. Male ($n=34$) and female ($n=2$) C57BL/6J mice between 13 and 26 weeks of age were used, except for one mouse aged 46 weeks. A total of 36 C57BL/6J mice were used ($n=10$ saline, $n=26$ SAH). One animal was excluded from the study because of a recording failure at the time of needle insertion and saline injection.

Anterior Prechiasmatic Injection Model of SAH

We used an injection model that has been described previously by our laboratory and others [12–14]. The anterior prechiasmatic injection model is advantageous because it allows for a titratable level of blood volume and injection velocity and leads to an early and persistent rise in intracranial pressure that recapitulates components of early brain injury [14, 15]. It differs from the endovascular perforation approach, which leads to an ischemic stroke (in addition to subarachnoid blood) and variable injury severity [16]. It is also distinct from cisterna magna injection models, which lead to blood in a more posterior location, relatively distant from the main cranial vault where the cerebral cortex resides in mice [17]. Mice were assigned to blood or saline at random. Blinding during the experiment was not possible. On each experimental day, both blood and saline injections were performed, and the order in which they were performed were varied to minimize potential confounding. Spontaneously breathing mice were placed under isoflurane anesthesia (3% induction and 1.5–2% maintenance in 70% N_2O/30% O_2 gas mix) and head fixed in a stereotaxic frame. Lubricating ointment was applied to the eyes. A homeothermic heating pad was set to 37 °C with feedback through a rectal probe. A midline incision was made to expose the frontal and parietal bones. Mineral oil was immediately applied to the dorsal surface to prevent drying and opacification of the skull. Further dissection of periosteum and other overlying connective tissue was performed, with care taken to reapply mineral oil as needed. Dissection and application of mineral oil was performed for approximately 5–10 min until the skull remained translucent. A burr hole was then drilled with a 0.7 mm drill bit (Drill Bit: Fine Science Tools Item No. 19007–07, Drill: Osada EXL-M40/LHP-12) overlying the right olfactory bulb, 5 mm anterior to bregma and adjacent to the midline, with care taken to avoid the frontal or sagittal venous sinuses. A spinal needle (Whitacre 27G, BD ref# 405079) containing either nonheparinized blood obtained through femoral artery cannulation from a littermate or normal saline was inserted through the burr hole at a 30–35° angle from the vertical axis. The needle was directed toward the midline to compensate for the off-center entry point. The needle was advanced approximately 7 mm until resistance was felt on contact with the base of the skull, and then the needle was retracted 0.5 mm. The mean ± standard deviation (SD) speed of needle advancement was 0.22 ± 0.09 mm/s for the saline group and 0.19 ± 0.09 mm/s for the SAH group ($p=0.48$). Following needle insertion, there was a variable time until injection of the syringe contents as described below. Isoflurane was decreased to 1%. Blood or saline (100 µl) was injected over 10 s with an electronically controlled injector (KD Scientific Legato 130 Syringe Pump, Holliston, MA, USA). The needle remained in place for the duration of image acquisition.

Imaging Setup and Analysis

A green LED (LEDD1B T-Cube LED Driver, M530L3 530 nm Green LED, ThorLabs, Newton, NJ, USA) and camera (ELP USBFHD06H-SFV USB Camera with 5–50 mm Varifocal Lens, Amazon.com) were positioned over the prepared skull (Fig. 1a). Imaging sessions were at least 5 min long. The camera was controlled with the Image Acquisition Toolbox in MATLAB (version R2018b MathWorks, Natick, MA, USA) with a final resolution of 920×780. Image acquisition for initial animals was at 15 frames per second (fps). Subsequent acquisition was at 30 fps to capture respiratory- and cardiac-influenced cerebral hemodynamic fluctuations. The LED was set to continuous illumination, and the intensity of light was adjusted to avoid overexposure or underexposure. The experimental preparation was isolated from ambient
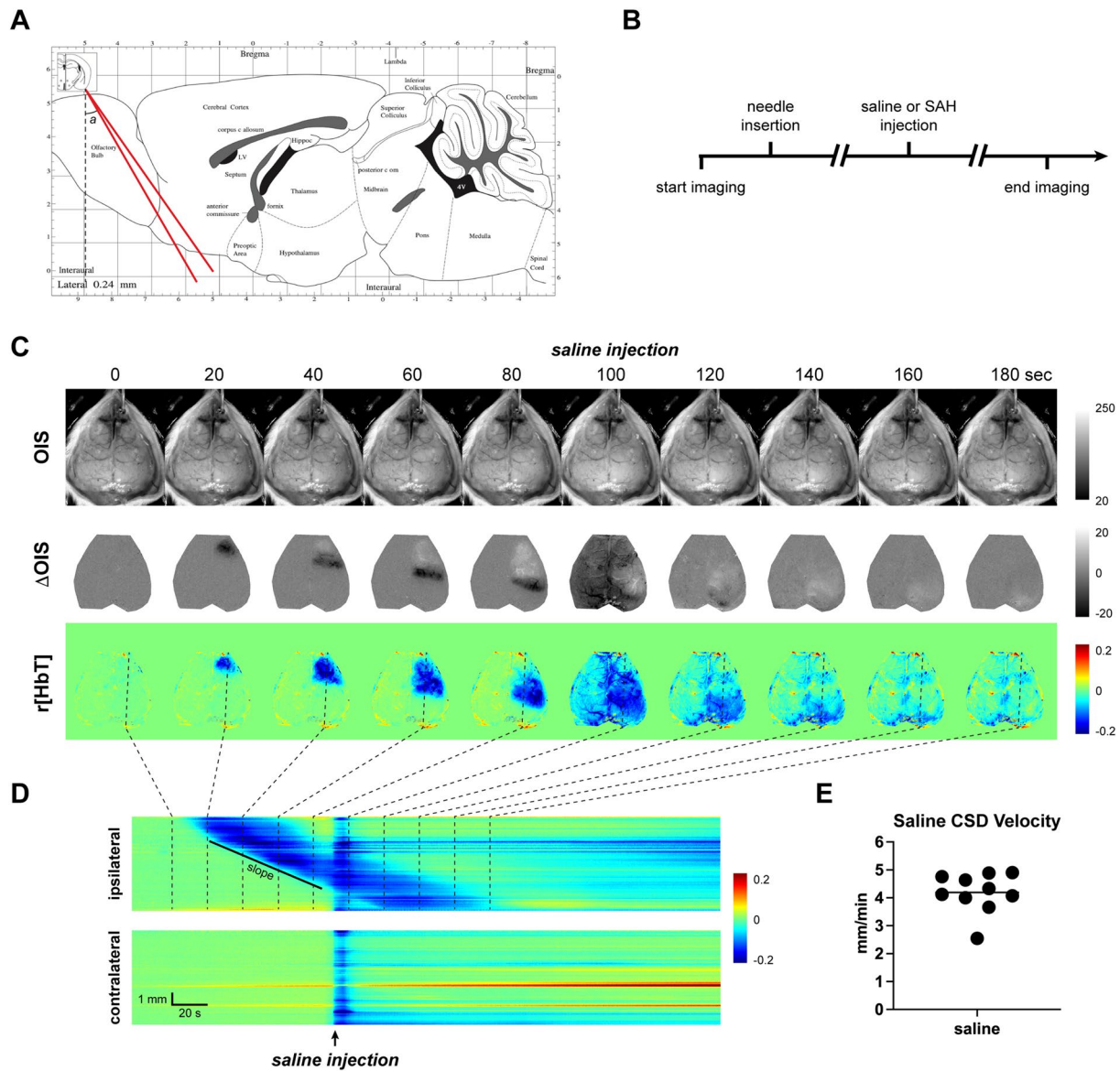
Fig. 1 Cortical spreading depolarizations (CSDs) occur following ipsilateral needle insertion. **a** Sagittal midline atlas adapted from Paxinos and Franklin showing injection needle insertion tract (red lines) over the olfactory bulb with a trajectory angle of 30–35° (**a**) from the vertical axis and a 6.5-mm needle advancement depth. **b** Experimental timeline. Imaging sessions were at least 5 min long. **c** Optical intrinsic signal (OIS), difference in OIS signal with a 10-s moving reference (ΔOIS), and change in total hemoglobin from a pre-CSD reference (r[HbT]) after needle insertion in a representative mouse. Time zero is the moment just before the appearance of a CSD. **d** Anterior–posterior line of interest shown in **c** plotted over time. The color scale corresponds to r[HbT]. The slope of the line across the CSD wavefront denotes the velocity of the CSD. **e** Velocity of CSDs calculated from the slope of the CSD wavefront following needle insertion in 10 mice subsequently injected with saline. SAH subarachnoid hemorrhage (Color figure online)

room light, and image acquisition was triggered prior to needle insertion. Data were analyzed by using a custom MATLAB script. To determine global hemodynamic fluctuations due to cardiac and respiratory activity, a region of interest was selected over the dorsal cerebral cortex reflectance images. The mean signal from the region of interest was determined for each frame and

then bandpass filtered at 1–10 Hz. In a separate analysis, the frame rate was reduced to 5 fps by using averaging with a convolutional filter over the time domain to reduce noise. A reference frame was chosen immediately following needle insertion to calculate relative changes in total hemoglobin concentration (r[HbT]). According to the modified Beer–Lambert law [18], change in total

hemoglobin concentration can be expressed as Δ[HbT] $(t) = -\log(I(t)/I_0)/(\varepsilon L)$, where "$I(t)$" is the green reflectance intensity at each pixel at the time (t), "I_0" is the reflectance intensity at the chosen reference time, "ε" is the extinction coefficient of hemoglobin at the isosbestic point of 530 nm, and "L" is the light pathlength through the tissue [19]. We assumed that optical pathlength "L" has the same value for all mice in our study and did not incorporate "ε" and "L" when calculating r[HbT]. Therefore, r[HbT] as used here is proportional to actual changes in total hemoglobin and was referred to in arbitrary units. Pixel to mm conversions were conducted by measuring the distance from the frontal sinus to lambda in pixels and normalizing to coordinates from the Paxinos and Franklin mouse brain [20]. To better visualize the progressing wavefront of CSDs, green reflectance images (i.e., optical intrinsic signal) were processed by taking the difference in optical intrinsic signal over a 10-s moving reference, as previously described [21]. Anterior–posterior lines of interest (LOIs) were selected on the basis of an r[HbT] frame post needle insertion and set to be parallel to the midline. Ipsilateral and contralateral LOIs were equidistant to the midline. Velocities of the CSD were calculated from the stabilized slope of the CSD wavefront on LOI r[HbT] time course plots (Fig. 1d). It was not possible to blind data analysis to SAH versus saline groups given visible blood seen following blood injections.

Statistics

Paired and unpaired t tests were performed with Prism 9 (GraphPad Software, San Diego, CA, USA). The threshold for statistical significance was a p value of < 0.05. All errors in the text and figures are in SD.

Results

There were CSDs in 100% of mice following needle insertion ($n = 36$ saline-injected and SAH-injected mice). CSDs occurred on the same side as needle insertion in all cases. The mean $\pm$ SD time delay between needle insertion and the appearance of the first CSD (CSD1) was

56 $\pm$ 8 s for the saline group and 58 $\pm$ 10 s for the SAH group ($p = 0.57$).

In saline control mice, there was 100% survival ($n = 10$). There were no subsequent second CSDs following needle insertion and saline injection (Fig. 1c, d). The average velocity of a CSD was 4.19 $\pm$ 0.71 mm/min (mean $\pm$ SD) (Fig. 1e), which is consistent with previously reported velocities [9].

In SAH mice, there was 88% survival ($n = 23$ of 26). A second ipsilateral CSD (CSD2$_{ips}$) to the CSD1 occurred in 31% (8 of 26) of SAH mice (Fig. 2a, b). The three mice that died also had CSD2$_{ips}$. In all cases, the origin of CSD2$_{ips}$ within the hemisphere differed from that of CSD1, and CSD1 and CSD2$_{ips}$ wavefronts propagated in opposite directions (Fig. 2a, b). Furthermore, CSD2$_{ips}$ was slower than the CSD1 (3.91 vs. 2.86 mm/min, $p = 0.0001$, $n = 8$, two-tailed paired t-test) (Fig. 2c). The remaining 69% (18 of 26) of mice had only one CSD ipsilateral to the needle injection site (Fig. 2c–e). The average propagation speed was no different from that of the CSD1 in those mice that went on to have two CSDs (3.90 vs. 3.91 mm/min, $p = 0.98$, $n = 18$ and 8, two-tailed unpaired t test). The time between the appearance of CSD1 (t_{CSD1}) and injection (t_{inj}) was varied to better visualize the temporal–spatial dynamics of CSD1. This variability was used to examine the relationship between t_{CSD1} and t_{inj} and the occurrence of CSD2$_{ips}$. A longer time interval between t_{CSD1} and t_{inj} was associated with the occurrence of CSD2$_{ips}$ in SAH-injected mice (26.4 vs. 72.7 s, $p < 0.0001$, $n = 18$ and 8, two-tailed unpaired t-test) (Fig. 2f). There were no instances of CSD2$_{ips}$ in saline-injected mice at any time interval ($n = 10$).

A second CSD occurred in the hemisphere contralateral to needle insertion (CSD2$_{contra}$) in a 16-week-old male mouse (1 of 26 SAH-injected mice) (Fig. 3). CSD2$_{contra}$ occurred following an early injection ($t_{inj} - t_{CSD1} = 28$ s; Fig. 2f) and appeared 182 s after CSD1. The CSD originated in a lateral location. No CSD2$_{contra}$ occurred in saline-injected mice ($n = 10$).

As expected, terminal CSDs were observed in the mice that died during imaging. Following CSD1 and subsequent SAH-associated CSD2$_{ips}$, there were CSDs in the

(See figure on next page.)
Fig. 2 Subarachnoid hemorrhage (SAH) injection can lead to multiple ipsilateral cortical spreading depolarizations (CSDs). **a** Optical intrinsic signal (OIS), difference in OIS signal with a 10-s moving reference (ΔOIS), and change in total hemoglobin from a pre-CSD reference (r[HbT]) images from a representative mouse in the SAH group that developed two CSDs ipsilateral to the needle insertion site. **b** Anterior–posterior line of interest versus time using the approach from Fig. 1d. The color scale corresponds to r[HbT]. The first CSD (CSD1) and second CSD (CSD2) on the ipsilateral side are indicated. The time when CSD1 is first observed (t_{CSD1}) and blood injection time (t_{inj}) are indicated on the plot. **c** Paired CSD velocities in mice for which there are two CSDs observed ipsilateral to needle insertion (+ CSD2$_{ips}$, open triangles). Closed triangles indicate CSD velocities in SAH-injected mice with only one ipsilateral CSD. **d** OIS, ΔOIS, and r[HbT] images from a representative mouse in the SAH group with only one CSD ipsilateral to the needle insertion site. **e** Anterior–posterior line of interest versus time in an SAH mouse with only one ipsilateral CSD. **f** A longer interval between the time when CSD1 is observed and blood injection time ($t_{inj} - t_{CSD1}$) is associated with the occurrence of a second ipsilateral CSD (CSD2$_{ips}$) for SAH-injected mice but not saline-injected mice. $n = 12$; second CSD, 8 of 12; survival, 9 of 12. SAH appears on the surface of the brain in the distribution of the middle cerebral artery (arrowheads) (Color figure online)
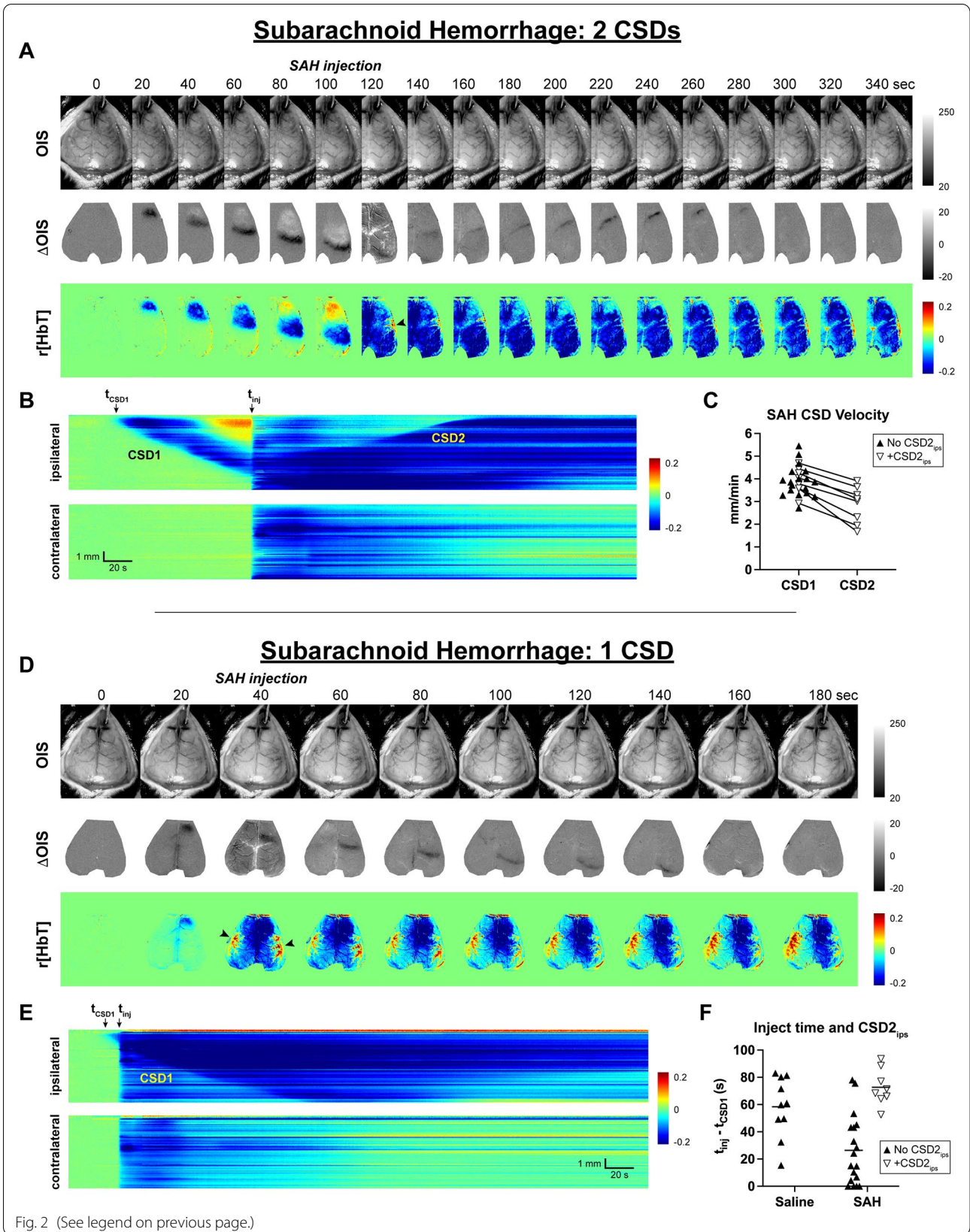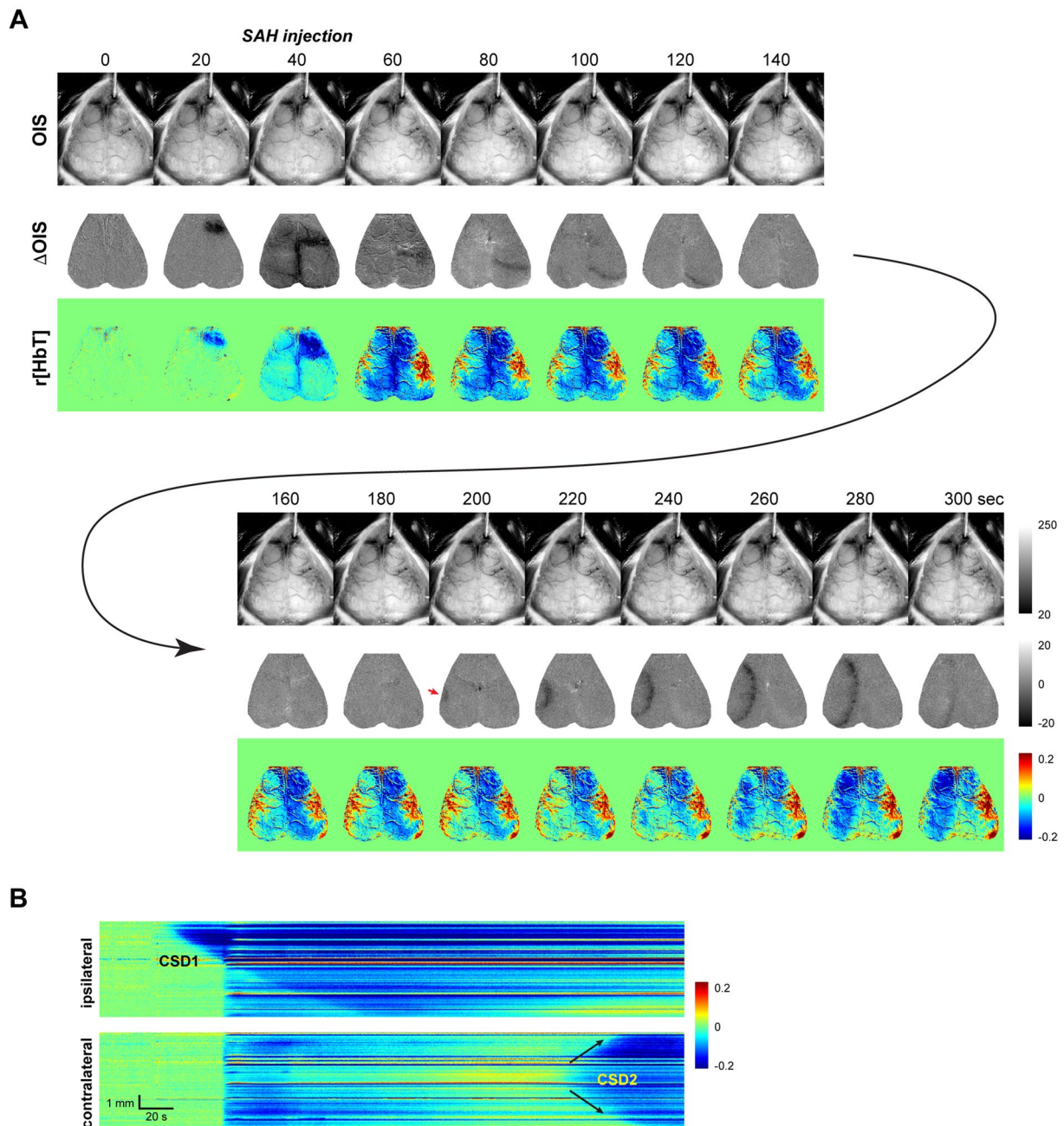
Fig. 2 (See legend on previous page.)

Fig. 3 Subarachnoid hemorrhage (SAH) injection can lead to bilateral cortical spreading depolarizations (CSDs). **a** Optical intrinsic signal (OIS), difference in OIS signal with a 10-s moving reference (ΔOIS), and change in total hemoglobin from a pre-CSD reference (r[HbT]) images from a mouse that developed a second CSD (CSD2) following SAH injection contralateral to the needle insertion site and first CSD (CSD1). A red arrow on the ΔOIS image at 200 s indicates the origin of the contralateral CSD2. **b** Anterior–posterior line of interest versus time. Arrows indicate anterior and posterior propagation of contralateral CSD2. The color scale corresponds to r[HbT]. $n = 1$ of 26 (Color figure online)

contralateral hemisphere appearing medially and laterally (Fig. 4a, b). Heart rate and respiratory rate were monitored with global signal variations (Methods) (Fig. 4c). We confirmed that terminal CSDs did in fact occur after cessation of respirations and pulse pressure variations.

Movies corresponding to representative images from all figures are included in the Supplemental Data.
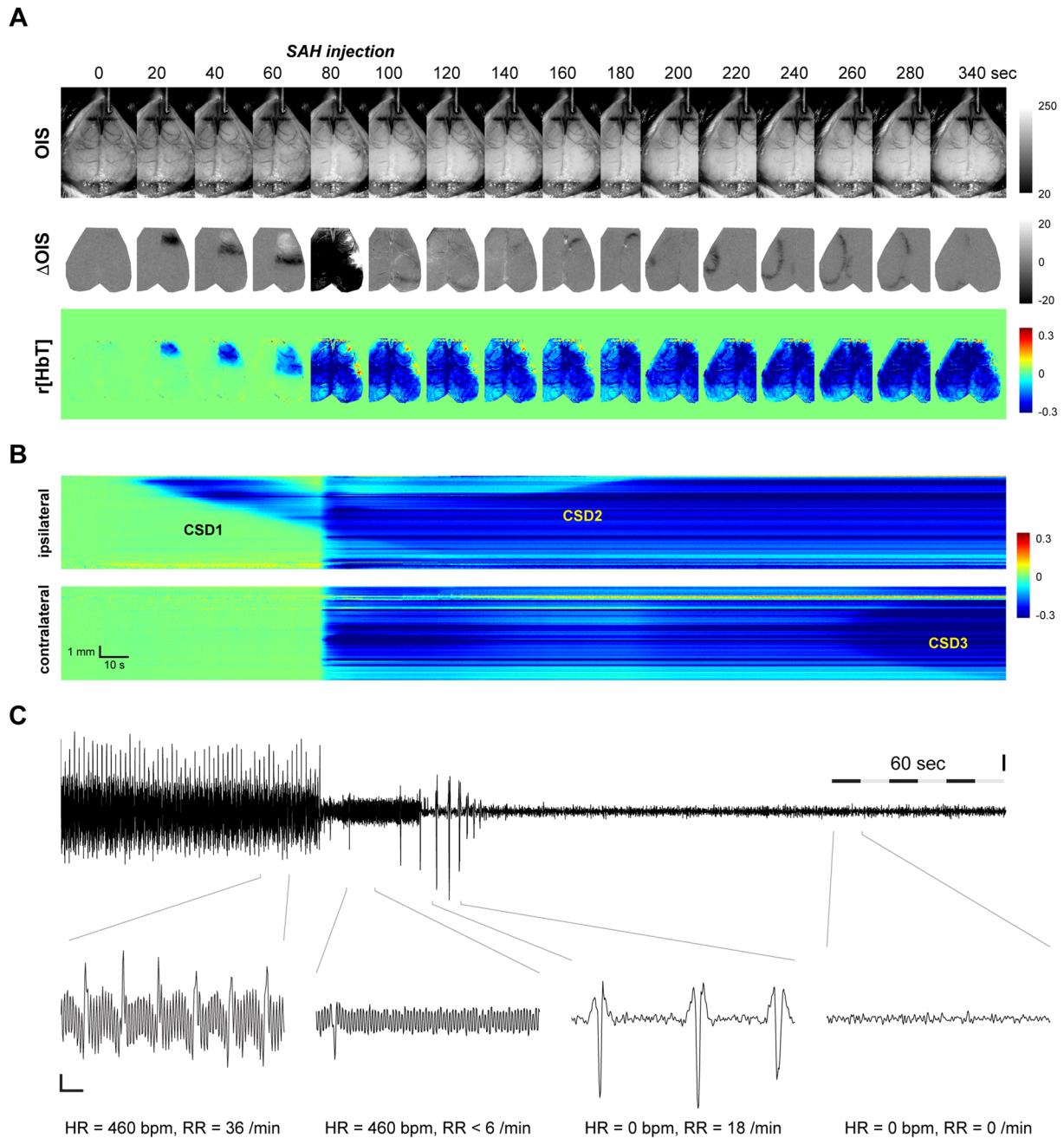
Fig. 4 Terminal cortical spreading depolarizations (CSDs) occur at the time of death. **a** Optical intrinsic signal (OIS), difference in OIS signal with a 10-s moving reference (ΔOIS), and change in total hemoglobin from a pre-CSD reference (r[HbT]) images from a mouse that developed two ipsilateral CSDs, had cardiac arrest, stopped breathing, and had a terminal contralateral CSD. **b** Anterior–posterior line of interest versus time. The color scale corresponds to r[HbT]. **c** The mean OIS signal over the masked dorsal brain surface, band-passed filtered to detect hemodynamic fluctuations due to heart contractions and respirations. The upper trace is aligned with **b** above. The vertical scale in the upper and lower traces are identical and in arbitrary units. There are four 10-s views in the lower panels detailing hemodynamic fluctuations and inferred heart rate (HR) and respiratory rate (RR). The lower horizonal scale bar is 1 s (Color figure online)

Discussion

CSDs are strongly associated with poor outcomes in patients with SAH. Whether CSDs cause poor outcome or are an epiphenomenon of a severely damaged brain is still unknown. Animal models will be essential in examining putative casual relationships between aneurysm

rupture, CSDs, and outcomes. Here, we find that the mouse anterior prechiasmatic injection model of SAH consistently includes a CSD following needle insertion through the olfactory bulb. Furthermore, in a subset of animals, we observe additional CSDs following blood injection but not following saline injection. The occurrence of subsequent CSDs is associated with the time between CSD1 and injection of blood.

Early in vivo CSDs have been observed in animal models of SAH but have never been previously reported in mice. We have recently summarized what has been learned about the relationship between CSD and SAH in these prior models for interested readers [7, 15]. Investigators using cat blood injection and arterial micropuncture models detected early CSDs using microelectrodes inserted in the brain [22, 23]. A recent report in a pig model observed CSDs and tissue ischemia acutely following blood clot placement in the subarachnoid space through a craniotomy [24]. There have been numerous rat studies using an endovascular perforation model of SAH, which detected CSDs in the acute phase with magnetic resonance imaging (MRI), cortical microelectrodes, or optical imaging through a craniotomy [25–28]. Bilateral CSDs were observed in two of these studies; diffusion-weighted MRI was used to detect CSDs in one of the studies [26], and the combination of MRI and microelectrodes was used in the other study [27]. To the best of our knowledge, there are no reports of CSD detection in rat prechiasmatic injection models. The only mouse study that attempted to observe CSDs did not see any spontaneous CSDs in the subacute (> 3 h) time period; however, the study was not designed to detect CSDs in the acute peri-SAH induction period [10]. The current study was designed to fill this gap in the literature by looking for CSDs just prior to and up to 5 min following SAH induction in a mouse model of the disease.

Our findings raise questions about the origin of CSDs in the prechiasmatic injection model of SAH. We did not expect to see CSDs on every needle insertion. Although pinprick is a well-known method for inducing CSDs [29], the needle insertion point for the anterior prechiasmatic injection model is through the olfactory bulb, which is anatomically distinct from the cerebral cortex in mice. There is, however, brain tissue in the caudal olfactory bulb (also known as dorsal olfactory bulb) that is histologically contiguous with the neocortical frontal pole [20]. A prior in vivo study on spreading depolarizations in the rat olfactory bulb observed occasional CSDs following potassium injection into the caudal olfactory bulb [30]. It is possible that needle insertion through the caudal olfactory bulb together with an area of structural continuity between the olfactory bulb and cortical frontal pole is enough to reliably induce CSDs. An alternative hypothesis is that the needle tip passed through cortical tissue or another structure at the base of the skull, which could have resulted in CSDs; however, it is unlikely for deep structure disruption to result in 100% CSD induction across so many animals. Future studies with in vitro brain slice electrophysiology experiments may provide additional insight into potential causes.

Another question is the mechanism of subsequent CSDs following blood injection. Why is there a second CSD on the same side as the initial CSD? Is it due to increased duration of ischemia from prolonged intracranial pressure elevation and reduced blood flow? Could it be due to direct blood irritation or release of extracellular potassium [24]? We also observed a delayed second CSD in the contralateral primary sensory cortex in one of the blood-injected mice. There is no clear explanation at this time, but perhaps a transient slowing of blood flow led to formation of microthrombi and subsequent focal ischemia [31]. The primary sensory cortex is thought to be particularly susceptible to CSDs in humans and mice [32]. Perhaps a global reduction in blood flow led to precipitation of a CSD in this vulnerable region. It is also interesting that CSD1 and $CSD2_{ips}$ travel in opposite directions of the CSD1. Perhaps the directionality is determined by the refractory period of post-CSD tissue. What is clear is that CSD1 is necessary for acute post-SAH CSDs to occur in our experimental paradigm because we did not observe additional CSDs at even very short $t_{inj} - t_{CSD1}$ times, before CSD1 passed through the hemisphere. Future work is required to better answer these questions and to precisely determine the conditions that predispose to post-SAH CSDs.

In light of our observations, there is a possibility that CSDs went undetected in previous rodent studies using the prechiasmatic injection approach. However, it is probably too early to reinterpret these earlier studies as being SAH plus CSD studies until further testing is conducted. For example, it is possible that CSDs produced by needle placement might not be seen in larger rodents, depending on the trajectory or final placement of the needle. Furthermore, the speed of needle placement and size of the needle may play a role in generating the initial CSD and should be examined in future studies.

The occurrence of second CSDs could be an additional source of experimental variability. The time from needle insertion to blood injection, which we find is a critical determinant to the number of CSDs in a particular animal, is not a commonly described variable in the literature and may not be noted by most experimentalists. Recording and reporting such details, including the number of CSDs seen in each mouse, may improve the predictive value of preclinical SAH research for translation to humans [33].

We recognize the burden of additional monitoring for CSDs in laboratories that do not routinely study the effect of CSDs. The approach described in the current study requires filtered light and custom MATLAB analysis scripts, which may not be feasible to develop or adapt by some investigators. We have, therefore, developed a convenient way to detect CSDs through intact mouse skulls in real time using an inexpensive USB camera and freely available analysis code in the hope of lowering the barrier to CSD detection by the wider community [21]. There is no doubt that experimental rigor could only be improved through such monitoring, at a minimum, to control for CSDs even in non-CSD-related studies.

Our study has the following additional limitations: (1) no blinding to saline versus. SAH injection, (2) few female mice included, (3) functional outcomes not reported, (4) only one mouse model assessed, and (5) observation for CSDs beyond 5 min not routinely performed.

Conclusions

CSDs occur in a commonly used mouse model of SAH at the time of needle insertion. The number of CSDs that occur in a given animal depends on the timing between the first CSD and blood injection. Noninvasive CSD detection in mice is feasible and should be considered in all mouse studies of SAH. Additional work is needed to determine the effect of CSDs on outcomes following SAH.

Supplementary Information

The online version contains supplementary material available at https://doi.org/10.1007/s12028-021-01397-9.

Author details

[1] Neurovascular Research Unit, Department of Radiology, Massachusetts General Hospital, Harvard Medical School, 149 13th St, Charlestown, MA 02129, USA. [2] Division of Neurocritical Care, Department of Neurology, Massachusetts General Hospital, Harvard Medical School, Boston, MA 02114, USA. [3] Athinoula A. Martinos Center for Biomedical Imaging, Department of Radiology, Massachusetts General Hospital, Charlestown, MA, USA. [4] Stroke Service, Department of Neurology, Massachusetts General Hospital, Harvard Medical School, Boston, MA, USA.

Data availability

The data of this study are available from the corresponding author on request.

References

1. Diringer MN, Bleck TP, Claude Hemphill J 3rd, et al. Critical care management of patients following aneurysmal subarachnoid hemorrhage: recommendations from the Neurocritical Care Society's Multidisciplinary Consensus Conference. Neurocrit Care. 2011;15(2):211–40.
2. Connolly ES Jr, Rabinstein AA, Carhuapoma JR, et al. Guidelines for the management of aneurysmal subarachnoid hemorrhage: a guideline for healthcare professionals from the American Heart Association/American Stroke Association. Stroke. 2012;43(6):1711–37.
3. Chung DY, Abdalkader M, Nguyen TN. Aneurysmal subarachnoid hemorrhage. Neurol Clin. 2021;39(2):419–42.
4. Fujii M, Yan J, Rolland WB, et al. Early brain injury, an evolving frontier in subarachnoid hemorrhage research. Transl Stroke Res. 2013;4(4):432–46.
5. Macdonald RL. Delayed neurological deterioration after subarachnoid haemorrhage. Nat Rev Neurol. 2014;10(1):44–58.
6. Chung DY, Oka F, Ayata C. Spreading depolarizations: a therapeutic target against delayed cerebral ischemia after subarachnoid hemorrhage. J Clin Neurophysiol. 2016;33(3):196–202.
7. Sugimoto K, Chung DY. Spreading depolarizations and subarachnoid hemorrhage. Neurotherapeutics. 2020;17(2):497–510.
8. Harriott AM, Takizawa T, Chung DY, Chen SP. Spreading depression as a preclinical model of migraine. J Headache Pain. 2019;20(1):45.
9. Ayata C, Lauritzen M. Spreading depression, spreading depolarizations, and the cerebral vasculature. Physiol Rev. 2015;95(3):953–93.
10. Oka F, Hoffmann U, Lee JH, et al. Requisite ischemia for spreading depolarization occurrence after subarachnoid hemorrhage in rodents. J Cereb Blood Flow Metab. 2017;37(5):1829–40.
11. Percie-du-Sert N, Hurst V, Ahluwalia A, et al. The ARRIVE guidelines 2.0: updated guidelines for reporting animal research. PLoS Biol. 2020;18(7):e3000410.
12. Sabri M, Jeon H, Ai J, et al. Anterior circulation mouse model of subarachnoid hemorrhage. Brain Res. 2009;1295:179–85.
13. Sabri M, Ai J, Lakovic K, et al. Mechanisms of microthrombi formation after experimental subarachnoid hemorrhage. Neuroscience. 2012;224:26–37.
14. Chung DY, Oka F, Jin G, et al. Subarachnoid hemorrhage leads to early and persistent functional connectivity and behavioral changes in mice. J Cereb Blood Flow Metab. 2021;41(5):975–85.
15. Oka F, Chung DY, Suzuki M, Ayata C. Delayed cerebral ischemia after subarachnoid hemorrhage: experimental-clinical disconnect and the unmet need. Neurocrit Care. 2020;32(1):238–51.
16. Parra A, McGirt MJ, Sheng H, et al. Mouse model of subarachnoid hemorrhage associated cerebral vasospasm: methodological analysis. Neurol Res. 2002;24(5):510–6.
17. Provencio JJ, Swank V, Lu H, et al. Neutrophil depletion after subarachnoid hemorrhage improves memory via NMDA receptors. Brain Behav Immun. 2016;54:233–42.
18. Ma Y, Shaik MA, Kim SH, et al. Wide-field optical mapping of neural activity and brain haemodynamics: considerations and novel approaches. Philos Trans R Soc Lond B Biol Sci. 2016;371(1705):20150360 (**Erratum in: Philos Trans R Soc Lond B Biol Sci. 2017;372(1714):20160539**).
19. Kohl M, Lindauer U, Royl G, et al. Physical model for the spectroscopic analysis of cortical intrinsic optical signals. Phys Med Biol. 2000;45(12):3749–64.

20. Paxinos G, Franklin KBJ. The mouse brain in stereotaxic coordinates. 2nd ed. San Diego: Academic Press; 2001.

21. Chung DY, Sugimoto K, Fischer P, et al. Real-time non-invasive in vivo visible light detection of cortical spreading depolarizations in mice. J Neurosci Methods. 2018;309:143–6.

22. Levitt P, Wilson WP, Wilkins RH. The effects of subarachnoid blood on the electrocorticogram of the cat. J Neurosurg. 1971;35(2):185–91.

23. Hubschmann OR, Kornhauser D. Cortical cellular response in acute subarachnoid hemorrhage. J Neurosurg. 1980;52(4):456–62.

24. Hartings JA, York J, Carroll CP, et al. Subarachnoid blood acutely induces spreading depolarizations and early cortical infarction. Brain. 2017;140(10):2673–90.

25. Busch E, Beaulieu C, de Crespigny A, Moseley ME. Diffusion MR imaging during acute subarachnoid hemorrhage in rats. Stroke. 1998;29(10):2155–61.

26. Beaulieu C, Busch E, de Crespigny A, Moseley ME. Spreading waves of transient and prolonged decreases in water diffusion after subarachnoid hemorrhage in rats. Magn Reson Med. 2000;44(1):110–6.

27. van den Bergh WM, Zuur JK, Kamerling NA, et al. Role of magnesium in the reduction of ischemic depolarization and lesion volume after experimental subarachnoid hemorrhage. J Neurosurg. 2002;97(2):416–22.

28. Shimizu T, Hishikawa T, Nishihiro S, et al. NADH fluorescence imaging and the histological impact of cortical spreading depolarization during the acute phase of subarachnoid hemorrhage in rats. J Neurosurg. 2018;128(1):137–43.

29. Pietrobon D, Moskowitz MA. Chaos and commotion in the wake of cortical spreading depression and spreading depolarizations. Nat Rev Neurosci. 2014;15(6):379–93.

30. Amemori T, Gorelova NA, Bures J. Spreading depression in the olfactory bulb of rats: reliable initiation and boundaries of propagation. Neuroscience. 1987;22(1):29–36.

31. Nozari A, Dilekoz E, Sukhotinsky I, et al. Microemboli may link spreading depression, migraine aura, and patent foramen ovale. Ann Neurol. 2010;67(2):221–9.

32. Bogdanov VB, Middleton NA, Theriot JJ, et al. Susceptibility of primary sensory cortex to spreading depolarizations. J Neurosci. 2016;36(17):4733–43.

33. Landis SC, Amara SG, Asadullah K, et al. A call for transparent reporting to optimize the predictive value of preclinical research. Nature. 2012;490(7419):187–91.